



ENHANCING THE RACKING RESISTANCE OF TIMBER SHEAR WALLS WITH STRUCTURAL GLASS: AN EXPERIMENTAL AND COMPUTATIONAL STUDY

Tine Engelen^{1,2,3}, Dries Byloos¹, Bram Vandoren¹

ABSTRACT: This work analyses the behaviour of structural timber-glass wall elements by carrying out experimental shear wall tests and calibrating a finite element model. Hybrid timber-glass diaphragms are a novel structural solution to increase the in-plane stiffness of façades in timber frame buildings. The solution is particularly interesting when large glass façades are desired in buildings with fewer inner structural walls. Therefore, this study investigates a hybrid system that activates the stiffness of the glass windows, using a structural silicone adhesive, to increase the structural stability of the timber façade. For these timber-glass systems, no existing design codes are applicable. A finite element model is developed in this contribution, simulating the mechanical behaviour of the system, including the timber-glass connections. This model is calibrated using small-scale connection tests. Additionally, eight shear experiments are performed on timber-glass façade elements to evaluate the strength and stiffness of the system. The behaviour of the various materials and connections is precisely captured using multiple measurement techniques, including Fibre Bragg Gratings embedded in the glass panes, Digital Image Correlation, and strain gauges. The experimental results are compared to the numerical model to assess its suitability.

KEYWORDS: Timber, Glass, Shear-wall, Adhesive, Photovoltaics

1 – INTRODUCTION

The structural design of timber structures includes the analysis of the horizontal stability, the so-called racking resistance, of the wall elements. Sufficient stiffness in timber buildings has to be created by combining façade wall elements and stiff interior structures. Within the design of modern timber buildings, the flexibility towards the future use of these structures is reducing the use of stiff inner structural walls. Therefore, the stiffness of façade elements will become increasingly important. Alongside this requirement, enough transparency is desired in buildings, which can be achieved by using large glass surfaces in façades. However, this conflicts with the need for stiffness in the façade. Therefore, this study proposes to use the strength and stiffness of glass to enhance the stiffness of timber frame wall elements by employing a structural connection between the timber frame and glass. Additionally, the energetical independence of these buildings can be further increased by including photovoltaic cells in the glass in areas where transparency is less necessary or not desired. This study investigates the mechanical behaviour of the multifunctional timber-glass system with integrated photovoltaics.

Previous studies pointed out adhesives as a good candidate for the structural connection between glass and timber [5, 7, 8]. Silicones maintain a good balance between flex-

ibility and strength, which is needed to avoid stress concentrations in glass and to activate the structural contribution of glass. Additionally, structural silicones have better weathering resistance than, for example, polyurethane and epoxy adhesives [4]. Therefore, this work uses a silicone adhesive to connect timber to glass, a detailed description of the proposed system is given in Section 2.1. The steps are taken in this work to understand the behaviour of the timber-glass structures. Firstly, different components of the system are characterised in detail with small-scale connection tests. Section 3.1 shows the results of push-out tests on the screwed timber-timber connections. Additionally, in a previous study by Engelen [2], the strength, stiffness and failure behaviour of the adhesively bonded timber-glass connections were evaluated and used to calibrate hyper-elastic material models. Secondly, an experimental test setup is developed to investigate the strength and stiffness of the proposed structure (Section 2.2). Using various measurement methods, including fibre Bragg gratings (FBG), digital image correlation (DIC), strain gauges and LVDTs, the behaviour of the system's components is accurately captured and used to validate the numerical model. The results of the testing program are described in Section 3.2. Special emphasis is put on the observed failure mechanisms during the tests. Thirdly, a numerical finite element model is built using results from the previously performed small-scale experimental connection tests. The model is described in Section 2.3, and the results are compared to the experimentally measured load-displacement diagrams in Section 3.2.

¹Construction Engineering Research Group, Faculty of Engineering Technology, UHasselt, Belgium, tine.engelen@uhasselt.be

²EnergyVille, Thorpark, Belgium

³IMO-IMOMECE, UHasselt, Belgium

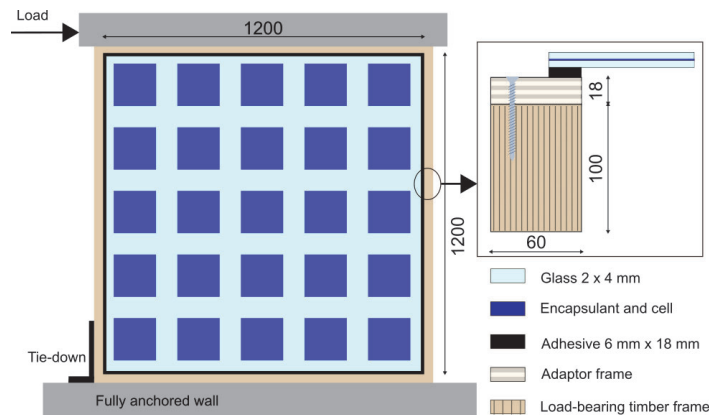


Figure 1: Timber-glass shear wall with a detailed cross-section (dimensions in mm)

2 – MATERIALS AND METHODS

2.1 MATERIALS

Experimental in-plane shear tests are performed on timber-glass composite structural elements with integrated photovoltaics. The timber frame is constructed with LVL timber (60 mm × 100 mm) and has a total width and height of 1.264 m. Laminated glass (including solar cells) is connected to this frame using an intermediate timber adaptor frame made of birch plywood with a thickness of 18 mm. This intermediate frame is screwed to the LVL timber frame, and the laminated glass is glued to the plywood frame using a structural silicone bond with a thickness of 6 mm and a width of 18 mm. In the test program, two types of two-component structural silicone are used to produce the specimen. A schematic representation of the specimen is shown in Fig. 1. Some specimens are equipped with a tie-down, anchoring the leading stud to the ground. These specimens are referred to as fully anchored, while the other specimens are partially anchored. In total, seven specimens were tested, four fully anchored and three partially anchored.

2.2 EXPERIMENTAL SETUP

The specimen is placed within a steel loading frame, as shown in Fig. 2. The bottom timber rail is connected to the testing frame using bolts (and a tie-down on the leading stud in case of a fully anchored system). Similarly, the top rail is connected to an overhead beam used for the load introduction. Out-of-plane movements of the top beam are restricted. A hydraulic cylinder introduces the load on the top left corner. The specimen is equipped with different LVDT sensors to measure the horizontal and vertical displacements of the timber and glass. Furthermore, a fibre Bragg grating (FBG) sensor is integrated into the glass to measure the strain on the photovoltaic solar cells [6]. On the four corners, on both sides of the glass, strain gauges (SG) are attached to measure the strains on the glass surface. Digital image correlation (DIC) is also used to capture the specimens' total strain and displacement field. Because of practical limitations, not all sensing techniques are used simultaneously. Therefore, Table 1 gives an overview of the different specimens, each with the used adhesive, type

of anchorage and used sensors.

Table 1: Overview of specimens: type of adhesive, type of anchorage and sensing (displacement sensors (LVDT), digital image correlation (DIC), fibre Bragg grating (FBG) and strain gauge (SG), Full anchorage implies the use of a tie-down at the leading edge of the frame)

Name	Adhesive	Anchorage	Sensors
Empty frame		Full	LVDT
K-DIC-P	Ködiglaze S	Partial	LVDT, DIC
K-SG-P	Ködiglaze S	Partial	LVDT, FBG, SG
K-DIC-F	Ködiglaze S	Full	LVDT, DIC
K-SG-F	Ködiglaze S	Full	LVDT, FBG, SG
D-SG-F	Dowsil™ 993	Full	LVDT, FBG, SG
D-DIC-F	Dowsil™ 993	Full	LVDT, DIC
D-FBG-P	Dowsil™ 993	Partial	LVDT, FBG

In addition, push-out tests on the adaptor frame to timber frame screws are performed. This gives information on the strength and stiffness of these connections. Six timber specimens, each with four screws of diameter 6.5 mm × and length 80 mm, are pushed until failure (Fig. 3). Each specimen is made of one central LVL block (60 mm × 100 mm × 200 mm), two plywood strips (60 mm × 18 mm × 200 mm) connected with two screws on each side. A vertical compression force is applied to the central LVL block.

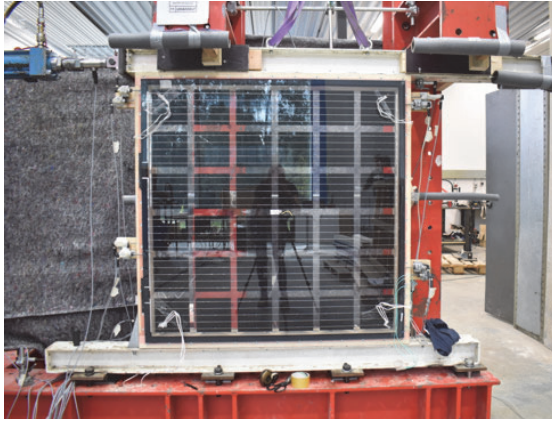


Figure 2: Test setup of the in-plane shear tests

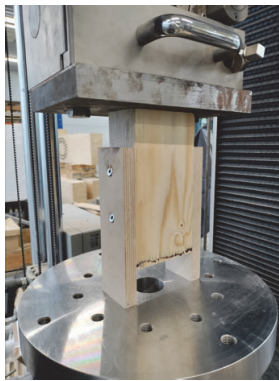


Figure 3: Test setup of the push-out test

2.3 FINITE ELEMENT MODEL

The behaviour of the specimen is predicted using the finite element software COMSOL Multiphysics. In this software, the complex material behaviour of the different materials can be represented using hyperelasticity, orthotropic behaviour and non-linearities. Table 2 gives an overview of the material properties used in the numerical model. An orthotropic linear elastic material model is used for the two types of timber (LVL and plywood). The correct fibre direction is applied for each component separately. The glass and encapsulant are modelled using linear elastic material models. Encapsulants have a time- and temperature-dependent behaviour, which can be represented using viscoelastic material models. However, for the current project, a linear approximation is used, and the encapsulant is represented using a thin (boundary) layer instead of a full 3D representation. This simplification is necessary due to the significant differences in aspect ratios within the model. The structural silicone adhesive is modelled using a hyperelastic material model with phase field damage. The incompressible neo-Hookean model uses a Lamé parameter μ of 0.781 MPa [2], and the damage model uses a principal stress criterion with a limiting stress of 2.5 MPa.

Furthermore, the screws and the tie-down are modelled using a steel material model with plasticity (Fig. 4 and Fig. 5). The bottom part of the tie-down is fixed. The yield strength for the screws is 500 MPa, and 250 MPa for the tie-

down, an isotropic hardening stiffness of 100 MPa is used. A thin layer (spring element) is applied between the stud and the tie-down representing the shear stiffness of the screws connecting the tie-down to the stud (18 screws of 4 mm \times 45 mm: $K = 11\,846$ N/mm). The stiffness is calculated using the Eurocode 5 [3] formula for the shear stiffness of screws: $K_{SLS,v} = 60 \cdot (d_1)^{1.7} \cdot (\rho_{\text{mean}}/420)^{1.1} \cdot 2 \cdot n_{\text{screws}}$, which is doubled because of the steel plate and multiplied by the number of screws. Rollers are applied on the side

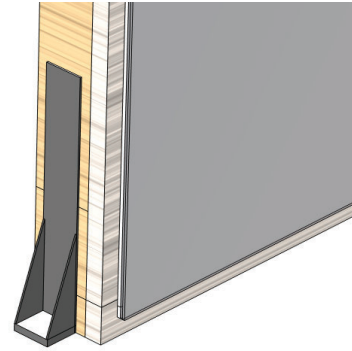


Figure 4: Numerical model: detail left bottom corner with steel tie-down

of the top rail, preventing out-of-plane displacements. The connection between the intermediate adaptor frame and the LVL timber frame is made with screws (diameter 6.5, spacing 100 mm). Instead of explicitly modelling each screw, a thin layer is used with a spring stiffness representing the shear stiffness of the screws. For this, the experimentally determined force-displacement curve, obtained from push-out tests, is used (see Section 3.1). Next, the screws connecting the rails to the studs are represented with a steel cylinder. To obtain the correct withdrawal stiffness, a thin layer is applied on the contact area of the screw and stud with a total stiffness of 5 kN/mm per screw (obtained from withdrawal tests). Finally, the bottom rail has a restricted negative displacement combined with spring foundation elements representing the stiffness of the bolts (obtained from tensile tests on the connection).

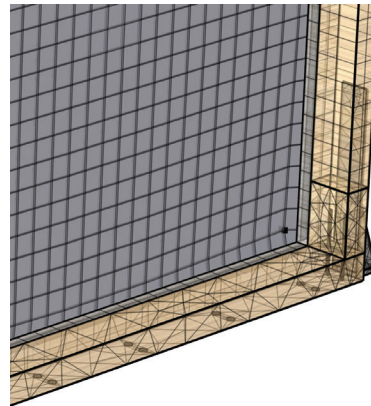


Figure 5: Finite element model: detail left bottom corner (from back side) semi-transparent, including the mesh

Table 2: Material properties used in the finite element model

	ρ [kg/m ³]	E [MPa]	ν [-]	G [MPa]
LVL S-beam	510	11600 - 350 - 100	0.4 - 0.2 - 0.2	400 - 1 - 270
Birch plywood	680	10048 - 7452 - 7452	0.4 - 0.2 - 0.2	206 - 183 - 183
Glass	2500	70 000	0.23	
Encapsulant	1760	10	0.4995	
Adhesive	1100	hyperelastic	0.49	
Steel	7850	200 000	0.3	

3 – RESULTS

3.1 RESULTS PUSH-OUT TESTS

Fig. 6 gives the average force-displacement per screw of the six tests and the mean value. The mean stiffness curve is used in the numerical software, determining the stiffness of the interlayer representing the screwed connection between the adaptor frame and the LVL frame. After the initial

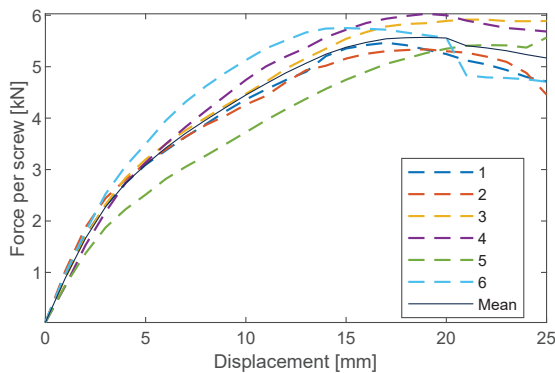


Figure 6: Push-out tests: force-displacement per screw

elastic domain, the stiffness of the connection is reduced due to the formation of a plastic hinge in the screws and compression of the timber. Finally, the LVL splits open in the plane of the screws (Fig. 7).

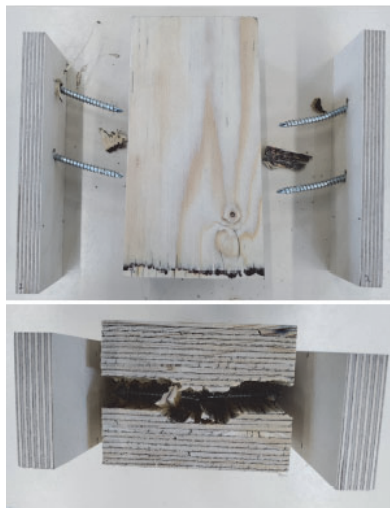


Figure 7: Push-out tests: failure modes of the tests

3.2 RESULTS IN-PLANE SHEAR TESTS

The results of the numerical model for the fully and partially anchored specimens are also shown in Fig. 8. A clear difference in stiffness is observed between the two models, caused by the tie-down. The numerical model is capable of predicting a reduction in stiffness due to progressive damage in the adhesive bond. In the experimental program,

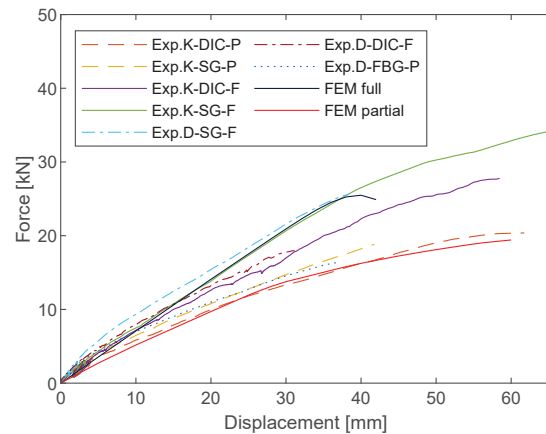


Figure 8: Experimental and numerical (comsol) force-displacement results

most specimens failed due to the rupture of the adhesive bond between the glass and timber. Failure started in the left bottom corner or top right corner, where the strain in the adhesive is the highest. For most specimens, the adhesive showed cohesive failure (Fig. 9a, 9c, 9d, 9e, 9i). However, some specimens with the Dowsil adhesive failed due to loss of adhesion to the timber surface (Fig. 9b). A suitable primer on the timber should be used to prevent this, as was done for the specimens with the other adhesive.

A second failure mode was the uplift of the left stud from the bottom rail. This uplift was small for specimens with a tie-down, while a significant uplift was observed for the partially anchored specimens (Fig. 9f). One specimen (K-SG-P) failed due to the withdrawal of the screwed stud-to-rail connection (Fig 9j). The latter specimen showed only limited adhesive failure.

Apart from the uplift from the stud to the rail, an uplift was observed during testing between the bottom rail and the support beam (Fig. 9h). After testing, it was visible on the back side of the frame that the bolts connecting the rail to the support frame had caused local deformations in the washer and timber (Fig. 9h). This was only observed for the partially anchored specimens and can be avoided by

using larger bolts and washers to avoid local crushing of the timber.

Furthermore, the shear forces were transferred from the main LVL timber frame to the adaptor frame via the screws, as tested in the push-out tests. Due to the number of screws used in the full-size diaphragm tests, the force and, thus, deformation per screw remained small. Therefore, the failure modes observed in the small-scale tests were not observed in the full-size tests.

The glass remained intact and attached to the timber frame in all tests. After the maximal force on the system was reached, a drop in stiffness was observed due to the adhesive rupture. However, some parts of the adhesive remained undamaged and were still able to carry the weight of the glass.

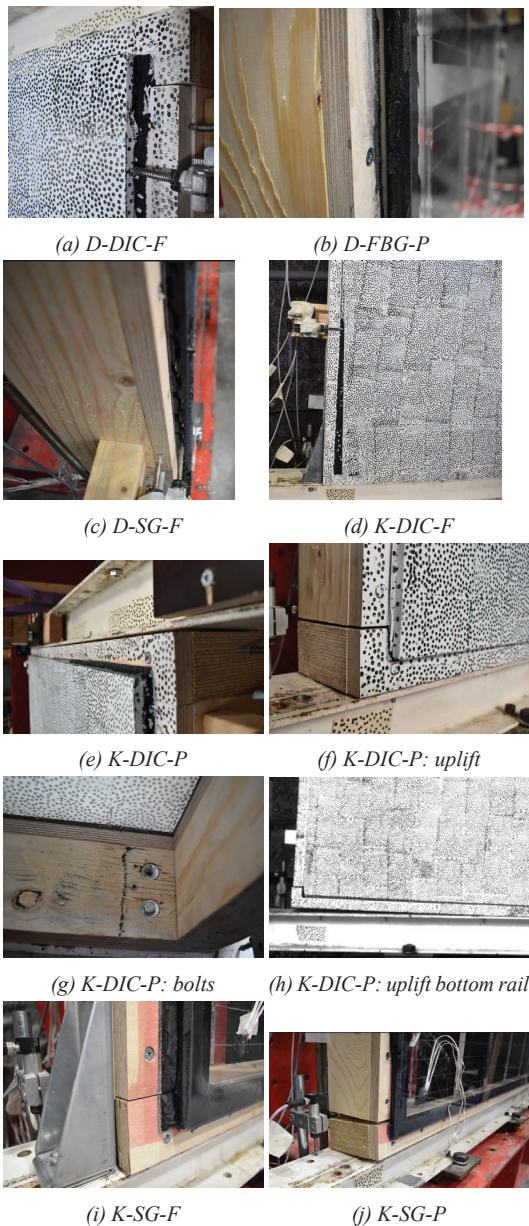


Figure 9: Failure modes of the specimen

The displacements in the system are captured using a DIC system. Fig. 10b gives the displacements measured using this DIC system for module D-DIC-F. The largest deformations occur in the adhesive bond, while the stiff glass panel has no significant deformations. The results are compared to the displacement field obtained in the finite element model in Fig. 10a.

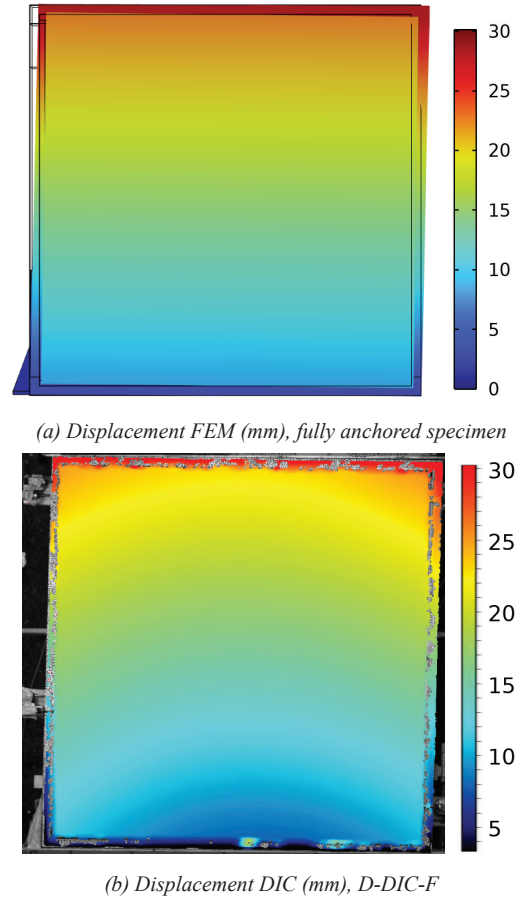


Figure 10: Displacement on fully anchored specimen: FEM vs DIC

In the experimental program, there was no glass breakage. However, to understand the glass panel's role in the system's stiffness, strains are measured on the glass. Fig. 11 indicates the principal strains measured on the four corners of the glass, both on the front and back side of the glass laminate. The back glass is attached to the timber frame with the adhesive, this causes a compression diagonal and a tension diagonal on the glass. It can be seen from the size of the arrows that the strain on the front side of the glass is smaller than the ones measured on the backside. This proves that there is a limitation in shear transfer through the interlayer between the two glass plates. A similar result is obtained when plotting the principal strains obtained in the numerical model (Fig. 12 and 13).

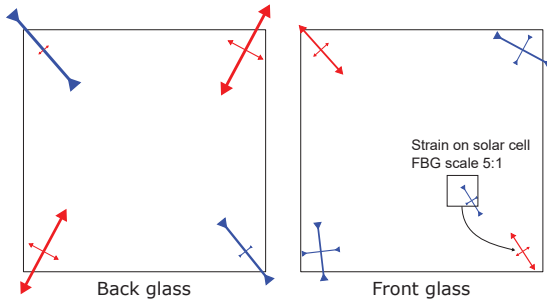


Figure 11: Experimental: principal strain: strain gauges K-SG-F at 15 kN

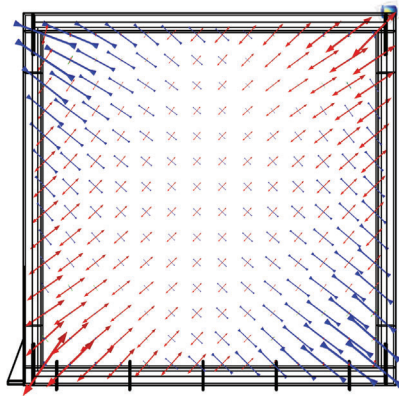


Figure 12: Principal strain directions back glass- Fully anchored specimen

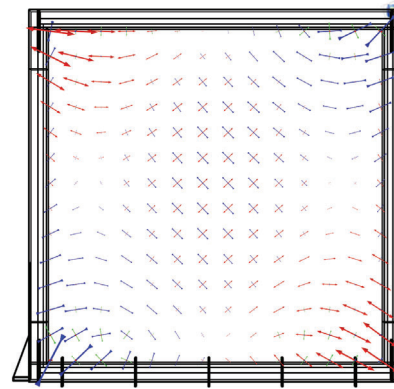
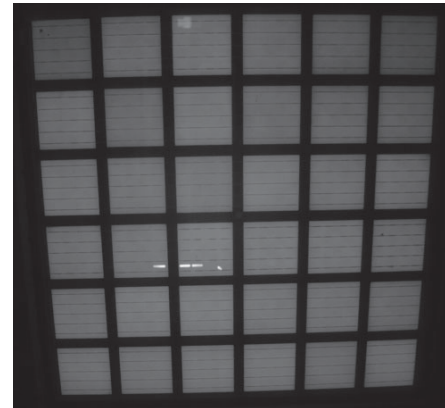
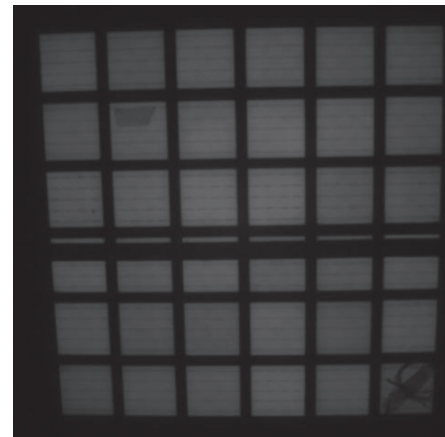


Figure 13: Principal strain directions front glass- Fully anchored specimen

Further, strain was measured using fibre Bragg gratings on the solar cell in the bottom right corner. In all modules, the maximal measured principal strain remained below $45 \mu\text{m/m}$. Additionally, electroluminescence (EL) is used to determine damage to the solar cells integrated into the glass before and after the experimental test. In this technique, a forward-biased PV module emits near-infrared radiation [1], which is captured with a camera with a special infrared lens. An undamaged PV cell lights up evenly, while a cracked solar cell would show dark regions. Only the silicon of the solar cell lights up, so dark lines on the cell due to metalisation and dark zones between the cells due to the spacing of the cells are expected. Fig. 14 shows the EL pictures before and after testing for module D-FBG-P. In the after figure, there are some visual obstructions: a safety belt to hold the glass in place, a label and some cables. The brightness of the two figures is a bit different due to external factors such as camera settings and daylight influence. Taking into account these limitations, no significant dark zones are visible in the figure before or after. This means the solar cell was not damaged during testing. Similar results are obtained for all tested modules.



(a) Before



(b) After

Figure 14: Electroluminescence: before and after testing. Important remarks: in the after picture, a belt is visible, which was in place for safety reasons, there is also a label (row 2, column 2) and some cables in the bottom right cell visible. The brightness of the figure can change due to camera settings

4 – CONCLUSIONS

The experimental and numerical program gives additional insights into the behaviour of structural timber-glass shear wall elements. The stiffness of the timber frame can be increased by structurally activating the glass with an adhesive connection. The design of this connection is important since the rupture of the adhesive bond was the main failure mode for the tested specimens. A further increase in stiffness can be achieved by anchoring the leading stud to the underlying structure with a tie-down. When this is not present, the withdrawal strength of the stud-to-rail connections should be considered an important failure mode, as was observed in the experimental campaign. When considering the maximal load on the system, it must be known that the rupture of the adhesive bond starts before the maximal force is obtained. Therefore, the design of such a system needs appropriate safety factors. The numerical model shown in this work is capable of predicting the overall stiffness behaviour of the system. In future work, this model will be further improved with more detailed connection models and validated against local measurements on the experimentally tested specimens.

Regarding the integration of photovoltaic cells in the glass, some interesting observations were made. Firstly, the strain, and thus also the stress, on the back glass was higher than on the front glass. This indicates that there is only limited transfer of shear forces through the interlayer. An FBG sensor on the solar cell indicated an even lower strain on the solar cell itself. This observation, together with the results of electroluminescence measurements, indicates that the solar cells were not damaged by the applied load on the system. The results of this study can be further used to refine the system's practical design guidelines and calculation methods.

ACKNOWLEDGEMENTS

The authors would like to recognize Dan Dragan and Niels Blocken for their contributions in conducting the experiments. They also extend their thanks to the Special Research Fund (BOF) of Hasselt University for its support of this research under Project Number BOF21DOC17. Special appreciation is given to Dow Silicones Belgium SPRL, especially Valerie Hayez and the laboratory team, for their invaluable assistance in specimen production and technical support. The authors express gratitude to Kömmerling Chemische Fabrik GMBH, particularly Christian Scherer and his team, for their insightful discussions and

help with specimen creation. Furthermore, they appreciate the contributions of Soltech NV and Tatjana Vavilkin in the production of solar panels, as well as DUPAC NV for supplying the necessary timber. Lastly, the authors acknowledge the experimental work of Jasper van Berlo and Ruben Wagemans related to their master's thesis.

REFERENCES

- [1] K. G. Bedrich. 'Quantitative electroluminescence measurements of PV devices'. PhD thesis. Loughborough University, 2017.
- [2] T. Engelen, J. Henriques and B. Vandoren. 'Experimental characterisation and calibration of hyperelastic material models for finite element modelling of timber-glass adhesive connections under shear and tensile loading'. In: *Glass Structures and Engineering* 9 (2024), pp. 551–568. DOI: <https://doi.org/10.1007/s40940-024-00268-x>.
- [3] European Committee for Standardization. *prEN 1995-1-1 Design of timber structures - General rules and rules for buildings*. CEN, 2025.
- [4] J. Giese-Hinz, C. Kothe, C. Louter and B. Weller. 'Mechanical and chemical analysis of structural silicone adhesives with the influence of artificial aging'. In: *International Journal of Adhesion and Adhesives* 117 (2022). ISSN: 01437496. DOI: 10.1016/j.ijadhadh.2021.103019.
- [5] D. Mocibob. 'Glass panel under shear loading-Use of glass envelopes in building stabilization'. PhD thesis. école polytechnique fédérale de Louvain, 2008.
- [6] P. Nivelles, L. Maes, J. Poortmans and M. Daenen. 'In situ quantification of temperature and strain within photovoltaic modules through optical sensing'. In: *Progress in Photovoltaics: Research and Applications* (2022). ISSN: 1099159X. DOI: 10.1002/pip.3622.
- [7] M. Premrov, A. Štrukelj and B. Ber. 'Experimental study on racking resistance of timber double-skin façade elements'. In: *Engineering Structures* 293 (2023). ISSN: 18737323. DOI: 10.1016/j.engstruct.2023.116712.
- [8] A. Štrukelj, B. Ber and M. Premrov. 'Racking resistance of timber-glass wall elements using different types of adhesives'. In: *Construction and Building Materials* 93 (2015), pp. 130–143. ISSN: 09500618. DOI: 10.1016/j.conbuildmat.2015.05.112.